DYNAMIC RESPONSE OF TURBULENT LOW EMISSIONS FLAMES AT DIFFERENT VORTEX BREAKDOWN CONDITIONS

F. Biagioli, B. Paikert, F. Genin, N. Noiray and S. Bernero
Alstom Power, Brown Boveri Strasse, 7. CH-5401, Baden, Switzerland

Abstract

Turbulent partially premixed flames stabilized at the Central Recirculation Zone (CRZ) produced via vortex breakdown of the reactants flow through a swirl burner are analysed here in order to determine their dynamic response to a small fluctuation of the inflow air mass flow rate. This problem is of particular interest in the thermoacoustic stability analysis of low emission gas turbine systems. It is shown via experiments and Large Eddy Simulation that vortex breakdown leads to two fundamental types of CRZ structures: type A) where the CRZ appears rather narrow in the radial direction with apex located close to the burner exit and type B), where the CRZ is entirely located in the combustor and appears more flat at its apex than observed for type A. Very different flame dynamic response (Flame Transfer Function, FTF) properties are observed for these two types of CRZ. Flames stabilized at the narrow CRZ (type A), respond to the inflow forcing with a time delay which depends much more on the bulk equivalence ratio than flames stabilized at the thick CRZ (type B). On the other hand the amplitude of the FTF in the case of the narrow CRZ state is in general lower and less sensitive to the bulk equivalence ratio than in case of the thick and flat CRZ state where amplification factors of the order of 4-5 are reached. Some qualitative explanations of the observed behaviour are provided.

1 Introduction

Modern heavy duty gas turbines can achieve very low levels of Nitrogen Oxides (NO_x) emissions by premixing fuel and air prior to combustion. Under optimized premixed conditions, stable anchoring of the flame is however more challenging than in conventional burners with highly non-premixed reactants. Acceptable premixed flame stabilization is usually ensured by adopting burners which give strong swirl to the stream of premixed reactants. This swirl leads, via the mechanism of vortex breakdown, to the formation of a Central Recirculation Zone (CRZ). In the region around the apex of the CRZ, where flow stagnation takes place, convective velocities are as low as the turbulent burning rate (i.e. the volumetric consumption rate of reactants for unit of turbulent premixed flame cross sectional mean area), the most favourable condition for flame anchoring to take place.

The operation of heavy duty lean premixed gas turbine combustion systems can be limited by combustion thermoacoustics instabilities. In this case fluctuations in acoustic velocity and pressure determine, via different mechanisms, fluctuations in the reactants flame consumption rate. The consumed reactants expand into up to two-three times less dense products, i.e. the flame acts as a source of gas volume generating acoustic waves and transferring energy into the acoustic field. The acoustic waves generated by the flame travel to the inlet and exit of the combustion system where they are eventually reflected back according to the local acoustic boundary conditions, producing additional fluctuations in the reactants consumption rate. A closed feedback loop between the acoustic field and unsteady consumption rate of reactants is in this way established. Thermoacoustic instabilities can be triggered depending on the phase and amplitude relation

between the acoustic field and the acoustically driven fluctuations in consumption of reactants (Rayleigh criterion [1]).

Thermoacoustic instabilities in heavy duty gas turbines occur with the excitation of acoustic modes having frequencies f comparable to the inverse of the convective residence time L_b/U_b in the burner and flame regions, i.e. Strouhal number $\simeq 1-2$, with L_b and U_b characteristic length and bulk velocity of the burner. Additionally to this, the Mach number $M = U_b/c$ is low, typically around $M = 0.1-0.2$, meaning that the acoustic wavelength is much larger than the characteristic dimension of burner and flame regions [2], i.e. $\lambda = c/f \simeq L_b\,(c/U_b) >> L_b$ (with c speed of sound). This has stimulated work in the past where acoustic wave propagation is considered one-dimensional along the main direction of the burner-combustor system and where the thermoacoustic stability analysis is performed, in closed loop mode, using network tools [3]. In this approach, the combustion system is decomposed in a series of elements (e.g. channel flow feeding air to the burner, fuel injectors, burner, flame, combustor, inlet and outlet), each of which is acoustically characterized via the response of the output pressure and velocity to a unit impulse in pressure and velocity at the inlet (Unit Impulse Response, UIR and, in the frequency domain, Transfer Function, TF). The stability analysis is performed in the liner regime according to closed loop control theory methods.

The flame represents the fundamental element of the thermoacoustic stability analysis. The flame static pressure drop scales as $\simeq M^2$, i.e. it is negligible at low Mach numbers typically found in gas turbine systems. The flame element is therefore acoustically characterized only via the link between downstream and upstream acoustic velocity fluctuations. The difference between these two is given by the fluctuation in the the production rate of hot gas volume (proportional to the heat release rate) driven by the acoustic forcing. Dynamic fluctuations in heat release rate are made of three main components: fluctuations in turbulent burning rate, in flame surface area and in hot gas density (due to unmixedness). Two main mechanisms have been proposed in the past generating these fluctuations: 1. due to fluctuations in equivalence ratio occurring at the location of fuel injection and reaching the flame after a given convective delay time [4], 2. due to fluctuations in the inflow reactants flow rate which are consumed (by the flame anchored at a fixed point, flame surface area mechanism) with a time delay equal to the mean residence time along the flame brush [5]. The Flame Transfer Function (FTF) represents in the frequency domain the relation in terms of phase shift ϕ (time delay $\tau \simeq d\phi/df$) and amplitude between the acoustic velocity upstream the flame and the volumetric production rate of products.

FTFs measured experimentally indicate physical mechanisms in gas turbine burners much more complicated than the ones mentioned above. Flame stabilization at the CRZ produced by vortex breakdown has been shown in [6] to have dynamic properties more complex than the case of flames stabilized at a fixed flameholder. Using Large Eddy Simulation, it was found in [6] that a very close relation exists between the FTF and the dynamic response of the CRZ to the inflow forcing. Assuming in fact the flame attached to the apex of the CRZ gave the opportunity to introduce a new mechanism for the dynamic production of hot gas volume. This consists in the consumption of reactants accumulated in the combustor volume and operated by the flame moving up and down with the CRZ. The time lag with which unsteady heat release respond to the acoustic perturbation was shown to be not the usual residence time along the flame brush but a larger one corresponding to the dynamic response of the CRZ apex to the inflow forcing.

The analysis in [6] was limited to fully premixed conditions and to a situation where the CRZ is localized in the combustor and appears rather flat at its apex. The structure of the CRZ can however quickly change in terms of the approaching flow as largely documented in the open literature [7]. For this reason in the first part of this work we assess, via experiments in a water

rig facility and Large Eddy Simulation (LES), the influence in a swirl burner of the approach flow on the structure of the CRZ produced via vortex breakdown. In relation to the thermoacoustic behaviour, the question that naturally arise is how the change in the structure of the CRZ affects the dynamic reponse of turbulent premixed flames stabilized via vortex breakdown. This is the subject of the last part of this work where experimental and numerical FTFs are presented and discussed.

2 Vortex breakdown of the flow through a swirl burner

Vortex breakdown is the fluid dynamics phenomenon where a Central Recirculation Zone (CRZ) is generated by imparting strong swirl to a given flow. Within the present work, the swirler discharges the flow into a duct followed by an expansion into the combustor (figure 1). The fully developed swirling flow generated by the swirler used here has a swirl number of approx 0.5. The phenomenology of swirling flows is well described by Batchelor [8] in terms of the Long-

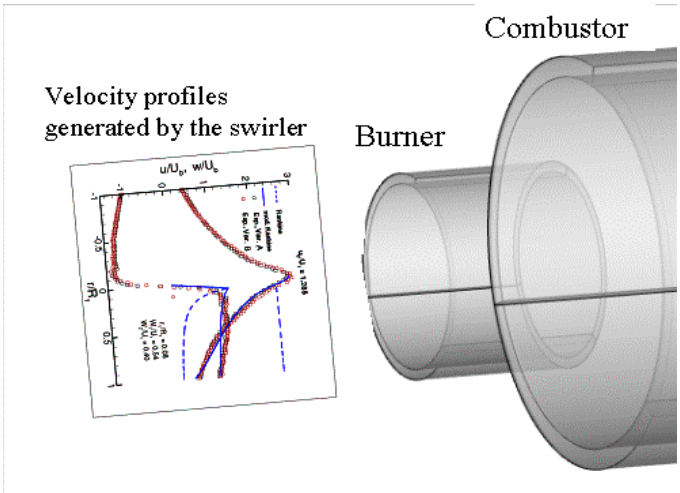

Figure 1: Schematic of the swirl burner followed by the combustor

Squire stream function equation under the assumption of inviscid, steady and axi-symmetric flow. This is given by

$$\frac{\partial^2\psi}{\partial x^2}+\frac{\partial^2\psi}{\partial r^2}-\frac{1}{r}\frac{\partial\psi}{\partial r}=r^2\frac{dH}{d\psi}-\Gamma\frac{d\Gamma}{d\psi} \tag{1}$$

where ψ satisfies $u = 1/r\,(\partial\psi/\partial r)$, $v = -1/r\,(\partial\psi/\partial x)$, such that $\nabla\psi\cdot\mathbf{u}=0$, i.e. the velocity vector lies on ψ isosurfaces (hence the name of stream function). This equation describes the evolution of azimuthal vorticity ω_θ (the lhs of the equation) for changes in flow cross sectional area in terms of the total pressure H and circulation Γ given as known functions of ψ for a given upstream generating vortex.

The effect of increasing the cross sectional area on a swirling flow is to diverge the streamlines with a reduction in tangential velocity (due to conservation of circulation). The streamlines rotate tangentially carrying with them the high axial vorticity contained in the rotational core. This gives production of a negative azimuthal vorticity component which, according to the Biot-Savart law, induces a negative variation in axial velocity at the axis and, eventually, leads to vortex breakdown. Intuitively, the higher the ratio between maximum axial and tangential tangential velocities u_0/w_{max} at the burner exit (i.e. the lower the swirl number), the higher is the final cross sectional area necessary for vortex breakdown. From a more rigorous point of view, the situation is well described by the Long-Squire equation (1). Under the assumption of quasi 1D flow (i.e.

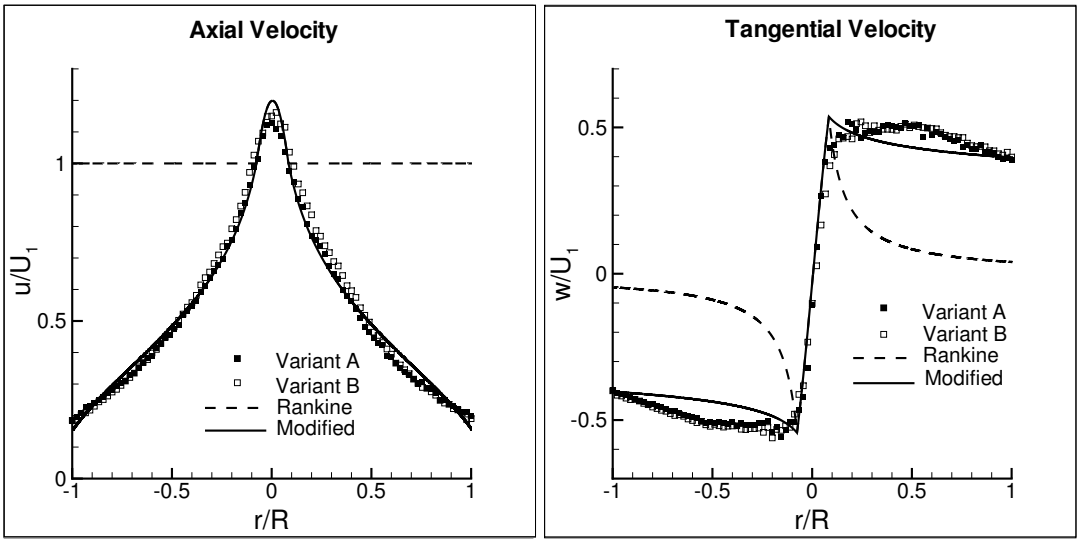

Figure 2: Experimental radial distributions of mean axial and tangential velocity in the burner. The figure shows also approximation with a Rankine and a modified Rankine vortices (the last not used here). Velocities are non-dimensionalised with the axial velocity at the boundary of the inner rotational core.

neglecting variations in the axial direction x), this equation admits analytical solution based on Bessel functions for an upstream generating vortex of the Rankine type, i.e. a vortex with uniform radial distribution of the axial velocity and with rigid body rotation $w = \Omega\, r$ in a inner core and irrotational $w \simeq 1/r$ outside this core.

Equation (1) has also been used by Keller [9] to study vortex breakdown. He allowed for the existence of a free lower boundary (representing the CRZ at $\psi = 0$) and used there the condition of constant static pressure. This gives stagnation along the all free bondary which becomes the boundary condition to use at $\psi = 0$ in equation (1). The solution, which is also analytical based on Bessel functions for an upstream generating vortex of the Rankine type, is not reported here but the method is used to get some preliminar information on the characteristics of the CRZ generated via vortex breakdown. The approximation of axial and tangential velocity radial profiles measured into the burner with the ones obtained from an optimized Rankine vortex from a larger cross sectional area is shown in figure 2. The figure shows that the Rankine vortex approximates well the experimental velocity distribution only in the inner rotational core. In the outer zone, the Rankine vortex is irrotational with uniform axial velocity while the experiments show weak rotationality and decreasing axial velocity. Given that vortex breakdown is mostly due to the strong axial vorticity in the rotational core which is well described by the Rankine vortex, the method can still provide useful information. Figure 3 right, shows the distribution of the lower free boundary versus increasing radius of the flow cross sectional area (conveniently transformed to an axial coordinate) obtained solving the quasi-1D form of equation (1) for equal increments of the peak axial velocity u_0 of the generating Rankine vortex. The CRZ is pushed downstream, as expected, with increasing u_0 and, the higher u_0, the more the position of the CRZ apex is sentive to the same variation δu_0.

This sensitivity is confirmed by the isocontour of mean zero axial velocity experimental obtained via Particle Image Velocimetry (PIV) in a water lab facility and shown in figure 3 left, for minor increments of a small amount of water mass flow rate (given in % of the total water flow rate) injected at the burner axis. A fast transition between two fundamental CRZ structures can be observed: type A, where the CRZ appears rather narrow in the radial direction with apex

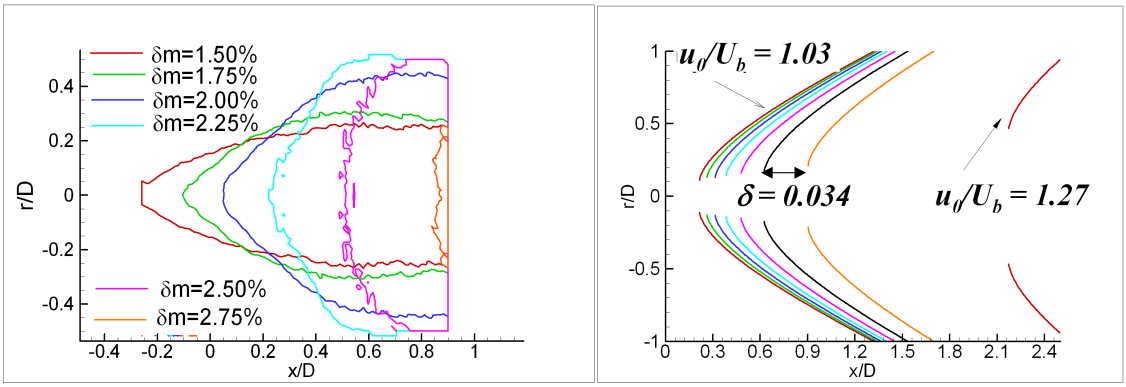

Figure 3: Left: PIV data, mean zero axial velocity contour in the combustor as function of small amount of water flow rate injected at the root of the burner, Right: free lower boundary from analytical solution of stream function equation (1) for increments of peak axial velocity u_0.

located close to the exit of the burner discharging the fully developed swirling flow into the combustor; type B, where the CRZ is entirely located in the combustor and appears more flat at its apex than observed in case of type A. A similar transition in the structure of the CRZ caused by vortex breakdown was also reported in the experimental work of Billant et al [7]. In that case, a fast variation between two types of CRZ was observed: a"bubble" shaped CRZ corresponding to the type A observed here and a "conical" shaped one orresponding to the present type B.

It is expected that the structure of the CRZ will play an important role in the static and dinamic behaviour of turbulent premixed flames stabilized via vortex breakdown. This aspect is analysed in the next section with experiments and Computational Fluid Dynamics (CFD). CFD is a powerful tool to shed light on complex flame-CRZ interaction mechanisms provided, however, that it is capable to capture the complexity seen so far experimentally. This point is investigated below.

The CFD analysis is based on the commercial (finite volumes) solver Fluent version 6.3.26. The mesh used is characterized by tetrahedral elements almost everywhere with exception of a cylindrical region covering the rotational part of the vortex core in the burner where hexahedral elements are used. The total mesh size is of the order of 2.8 millions elements. CFD is assessed in the form of Reynolds Averaged Navier-Stokes (RANS) equations based on the standard $k-\epsilon$ method and Large Eddy Simulation (LES) with standard Smagorisky turbulent model. The discretization of convective terms is based on the second order QUICK scheme in case of the RANS method and on a bounded central differencing scheme in case of the LES simulations. In the LES method the solution is advanced in time using second order discretization and a time step of approx 0.056 (non-dimensionalized with the bulk residence time in the burner). Averaging is performed over a time approx 20-30 times the bulk residence time.

CFD results are reported in figures 4-7. Despite the large differences observed in vortex breakdown structure, the differences in the approaching flow can be hardly recognized. The significant variation in the structure of the CRZ observed experimentally (figures 3 left and 5 from LDA analysis) takes place in fact only with minor changes in the characteristics of the approach flow as documented by figure 5 showing radial profiles of axial and tangential velocity in the burner.

From the CFD side, LES is well capable in capturing the radial velocity profiles inside the burner (figure 4) but the RANS method totally fails, underestimating the rigid body rotational speed close to the axis by approx a factor ten! The small rotational vortex core characterized by large velocity gradients (approx 10% of the total vortex size) doesn't in fact experimentally

diffuses in radial direction while it is an intrisic characteristic of the $k-\epsilon$ model do produce large "eddy diffusivity" as soon as large gradient in mean flow velocities are found.

In case of the RANS approach, it has been found that the mesh quality and refinement don't play a significant role, indicating that the problem is mostly controlled by (unrealistically) high radial diffusion of the $k-\epsilon$ model. In case of LES, the mesh quality was instead found to play an important role as it is expected due to physical diffusivities smaller than unrealistically high values of the RANS method.

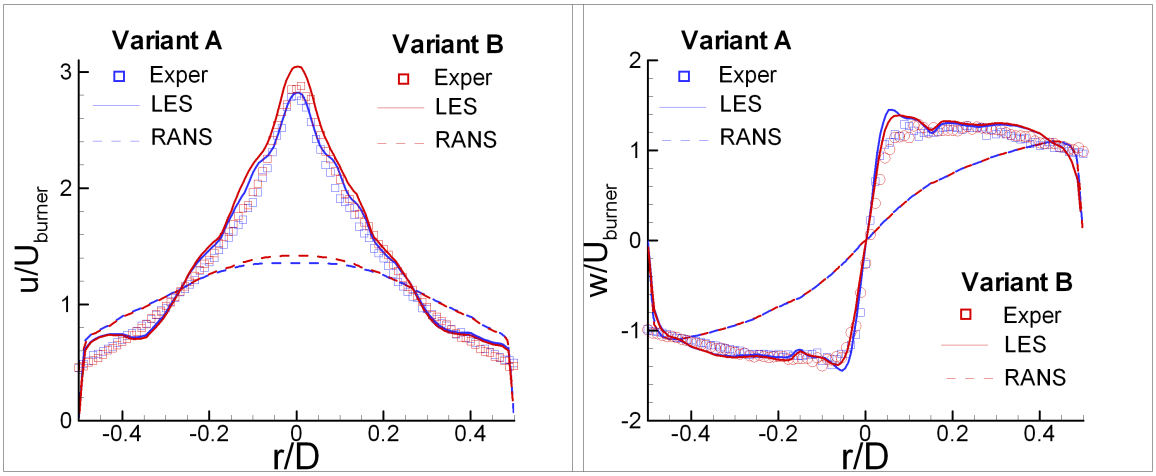

Figure 4: Comparison of mean axial and tangential velocity from RANS and LES with experimental data in the burner.

Isocontours of mean axial velocity shown in figure 5 for the region around the CRZ show a remarkable agreement between LES results and LDA data, a condition which gives confidence in being able to shed light on the flame dynamic behaviour via combusting LES analysis. Validation

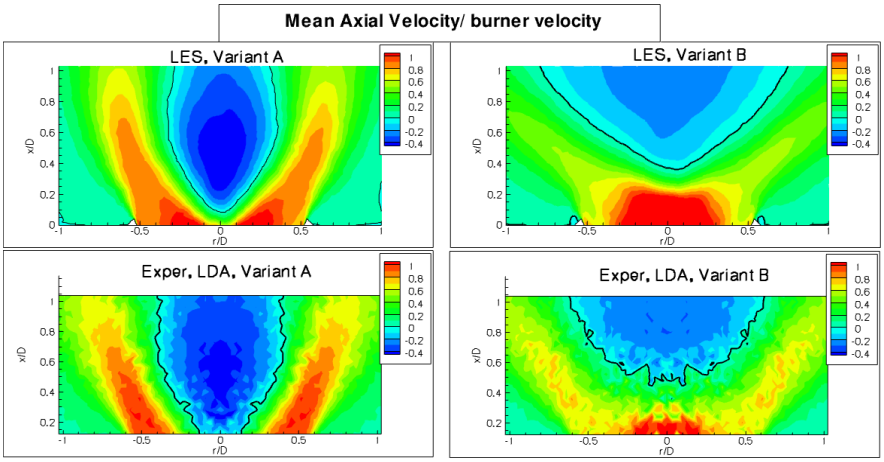

Figure 5: Mean axial velocity distribution for CRZ of type A and B. Comparison between experiments and LES

versus minor increaments of water flow rate at the axis are shown in figure 2. Radial profiles of mean axial velocity going through the apex of the CRZ are also shown. The figure confirms that LES can cope with this problem while the RANS $k-\epsilon$ method is not capable of predicting the sensitivity of the CRZ shape and position to the inflow conditions.

Additonal validation includes a comparison of coherent structures given from Proper Orthogonal Decomposition. Figure 7 shows good agreement between experimental data and LES for a vortex of type A in a small observation window close to the apex of the CRZ. In this case, approx 30% of the energy is contained in the first mode which correponds to an axial displacement of the CRZ. The second mode is also axial, contains approx 7% of the fluctuating energy and corresponds to a fluctuation in the slope of the velocity along the axis. The third mode is anti-symmetric and corresponds to precession.

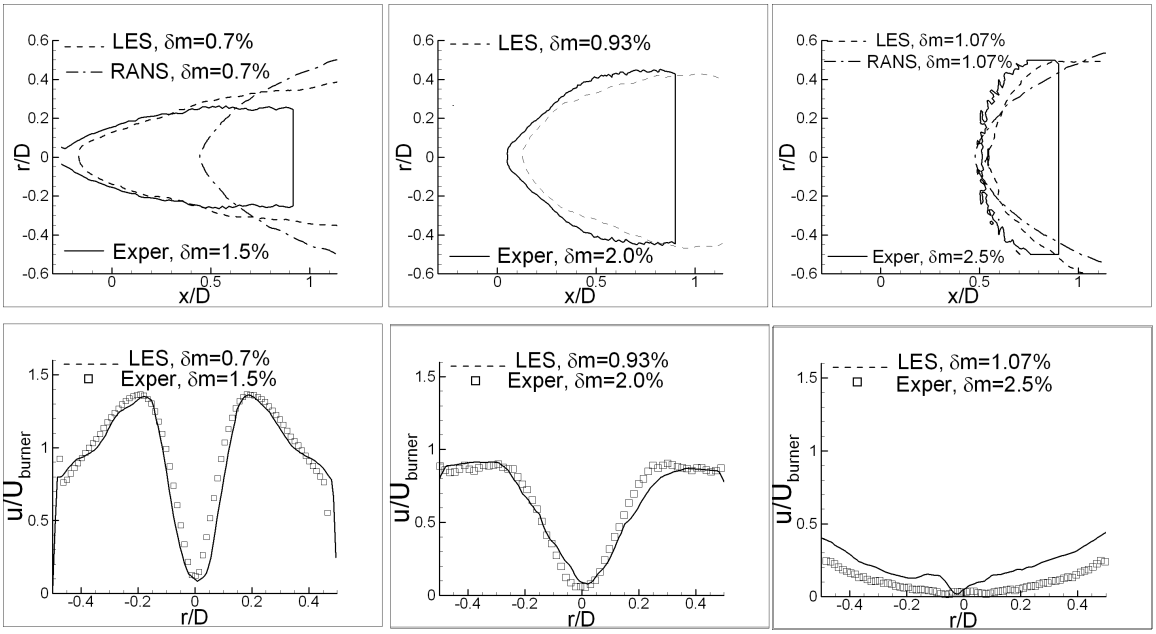

Figure 6: Radial profiles of mean and rms of axial and tangential velocities close to the apex of the cRZ for transition between type A and type B structures.

3 Static and dynamic properties of turbulent premixed flames stabilized at two different vortex breakdown structures.

The transfer matrix of the flame element in the thermoacoustic stability analysis based on network modelling reduces at low Mach number to the relation in frequency domain (phase shift and amplitude ratio) between an harmonic forced velocity perturbation just upstream of the flame and the velocity response just downstream. The difference between these two velocity is given by the volumetric production rate of hot gas (products). The response of this last quantity to the inflow forcing signal is known as Flame Transfer Function. LES simulations of turbulent partially premixed flames are based in the present work on the Turbulent Flame-Speed Closure originally developed by Zimont (TFC model [10]). This is based on the solution of the the following transport equation for a reaction progress variable c (Favre averaging):

$$\frac{\partial(\overline{\rho}\,\tilde{c})}{\partial t} \quad + \quad \nabla\cdot(\overline{\rho}\,\tilde{\mathbf{u}}\,\tilde{c}) = \nabla\cdot(\overline{\rho}\,D_t\nabla\tilde{c}) + \rho_u\,U_t \;\mid \nabla\tilde{c}\mid \tag{2}$$

where the turbulent burning rate U_t is modelled as $U_t = A\,u'\,Da^{1/4}$ with $A = 1$ proportionality constant, u' the turbulent velocity characteristic fluctation and Da the local Damköhler number. The relation between the area averaged axial velocities in front (section I) and behind the flame (section II) is obtained via integration of equation (2) and equation of total mass conservation as (mathematics not shown here, see [2]):

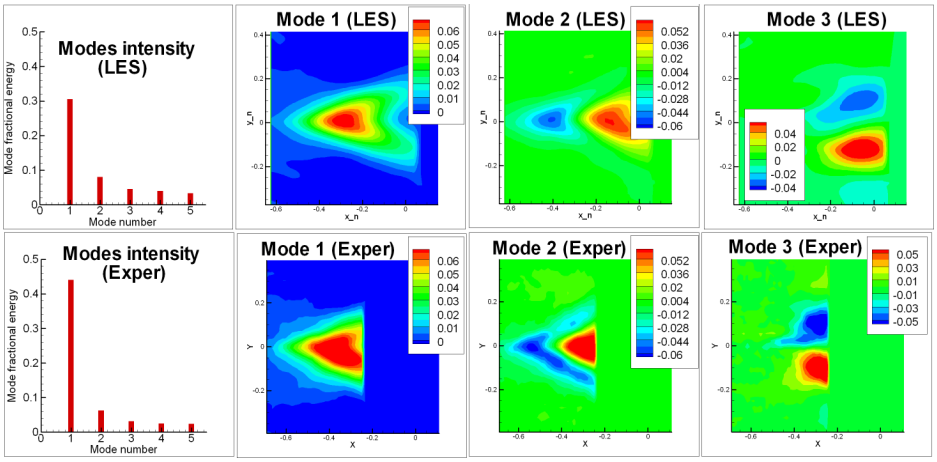

Figure 7: Distribution of POD modes in experiments and LES

$$U_{II} = U_I - \frac{\tau - 1}{A_{II}} \int_V U_t \mid \nabla \tilde{c} \mid dV \tag{3}$$

with $\tau = \rho_R/\rho_P$ ratio between densities in the reactants and products stream and volumetric reactants consumption rate given by $\dot{Q}_v = \int_V U_t \mid \nabla \tilde{c} \mid dV$.

The linearization of this equation yields the following result:

$$U'_{II} = U'_I + \frac{(\tau - 1)}{A_{II}} \dot{Q}'_v \Rightarrow \frac{U'_{II}}{U'_I} = 1 + (\tau - 1) \frac{\dot{Q}'_v / \overline{\dot{Q}_v}}{U'_I / \overline{U_I}} \tag{4}$$

where mass conservation $\overline{U_I}\, A_I = \overline{\dot{Q}_v}$ and $A_{II} = A_I$ have been used. In the LES simulations, the forced fluctuation U'_I is imposed via a small (5% of mean velocity) forced variation of inflow velocity U'_i at the inlet air boundary having area A_i. From mass conservation we have $U'_I/\overline{U_I} = U'_i/\overline{U_i}$ which can be replaced in the rhs of equation (4). The dynamic response of the flame is determined in "time domain" as the response $\dot{Q}'_v = h_Q(t)$ to a unit inpulse $U'_I = \delta(t) \Rightarrow U'_i = \delta(t)\, A_{II}/A_i$ (FTF in frequency space). Under strong turbulent conditions however excition with just an impulse is not sufficient for the identification of the dynamic response $h_Q(t)$. In the LES analysis, the identification is done using a Wiener-Hopf filtering technique [11]. The fluctuation of any variable $y(t)$ (e.g. $\dot{Q}'_v$) in the computational domain is decomposed as $y(t) = y^{(d)}(t) + y^{(t)}(t)$ where $y^{(d)}(t)$ and $y^{(t)}(t)$ indicate respectively the "dynamic" response to forcing and "turbulent" noise parts of $y(t)$. A forced velocity fluctuation $U'_i(t)$ containing energy in the frequency range of interest is then imposed at the air inlet. The relation between $y^{(d)}(t)$ and $U'_I(t) = U'_i\, A_i/A_{II}$ at the LES time t_n is given (in linear regime) by the convolution

$$y^{(d)}(t_n) = \sum_{l=1}^{L} h(\tau_l)\, U'_I(t_{n-l})\, \Delta t \tag{5}$$

The separation of $y^{(d)}(t)$ and $y^{(t)}(t)$ in $y(t)$ is determined in the Wiener-Hopf method by requiring that the dynamic part $y^{(d)}(t)$ minimizes the mean square error given by:

$$\min \left\{ E = \sum_{n=1}^{NT} \left[y(t_n) - y^{(d)}(t_n) \right]^2 = \sum_{n=1}^{NT} \left[y(t_n) - \sum_{l=1}^{L} (h(\tau_l)\, U'_I(t_{n-l})\, \Delta t \right]^2 \right\} \Rightarrow \frac{\partial E}{\partial h_l} = 0 \tag{6}$$

which leads to the solution of the following linear system of equations of dimensions $L \times L$:

$$\sum_{l=1}^{L} \left[\sum_{n=1}^{NT} U'_I(t_{n-l})\, U'_I(t_{n-k}) \right] h(\tau_l) = \sum_{n} y(t_n)\, U'_I(t_{n-k}), \qquad k = 1, 2, ..., L \tag{7}$$

Generally speaking, the larger the ratio between turbulent and dynamic contributions, the larger the number of time samples that are needed to determine the unit impulse response with sufficient accuracy. The length of the unit impulse response is also a parameter which needs to be conveniently determined.

Combustion experiments have been carried out in an atmospheric single burner test facility at the Alstom Test Center in Birr - Switzerland. The experimental determination of the FTF is based on a technique where forced excitation is provided via loudspeakers and the acoustic wave propagation in the channels before the burner (U'_I) and in the combustor (U'_{II}) is reconstructed from the pressure signal measured by a set of microphones [12]. Optical access via two air cooled quartz crystal windows allowed also for detection of the OH* concentration via chemiluminescence (CL) with an intensified CCD camera and for PIV laser velocity measurements. The CL-images give a qualitative idea of the displacement of the the flame front which is sufficient for the scope of the present work. Time averaging of the CL and PIV data was performed over approx 200 images.

The measurements have been carried out in presence of CRZs of both type A and type B and for different value of the bulk air excess factor. The static (mean) flame characteristics are presented in figures 8 (LES and experiments). Figure 8 right shows the time averaged CL intensity contour plots, normalized by the maximum CL intensity and the mean zero axial velocity isocontour (CRZ) obtained via PIV. In case of CRZ of type A, there is a clear upstream movement of the the maximum CL-intensity with decreasing air-fuel ratio. In the case of CRZ of type B, there is no significant movement of the maximum intensity or CRZ position. The precise behaviour of the type A - CRZ apex position is not clear from the PIV images given that it was not possible to measure inside the burner. The increase observed in the burner pressure drop for the CRZ of type A (and not for the one of type B) however supports the idea that the apex of the CRZ moves upstream together with the flame. Such a flame behaviour is confirmed by LES results as shown in figure 8 left. The calculated flame moves indeed upstream with decreasing air excess factor in case of CRZ of type A (and the CRZ apex as well) while it doesn't move in case of CRZ of type B.

The calculated and experimental FTFs (Fourier transform of the unit impulse response of hot gas production rate) are shown in figure 9. Both investigation methods shows that the phase delay between heat release and velocity forcing for CRZ of type A is more sensitive to the air excess factor than in case of CRZ of type B. Such sensitivity doesn't seem however to be due to a change in the time delay. The slope of the phase versus frequency (to which the time delay is proportional) doesn't in fact change significantly with λ both in the experiments and in the LES. A more plausible explanation consists instead in a change of the phase relation between forcing and heat release, i.e. in opposition of phase at the very lean conditions and in phase at the more rich ones.

The amplitude distributions of the FTF show that flames stabilized at the CRZ of type B tend to amplify acoustic energy more than flame stabilized at the CRZ of type A, especially at the most lean conditions. Amplitudes values of approx 6-7 are reached for rich conditions. Such high values cannot be in any way explained with the simple model of a flame anchored

©Copyright ALSTOM 2011. All rights reserved. Information contained in this document is provided without liability for information purposes only and is subject to change without notice. No representation or warranty is given or to be implied as to the completeness of information or fitness for any particular purpose. Reproduction, use or disclosure to third parties, without prior express written authority, is strictly prohibited.

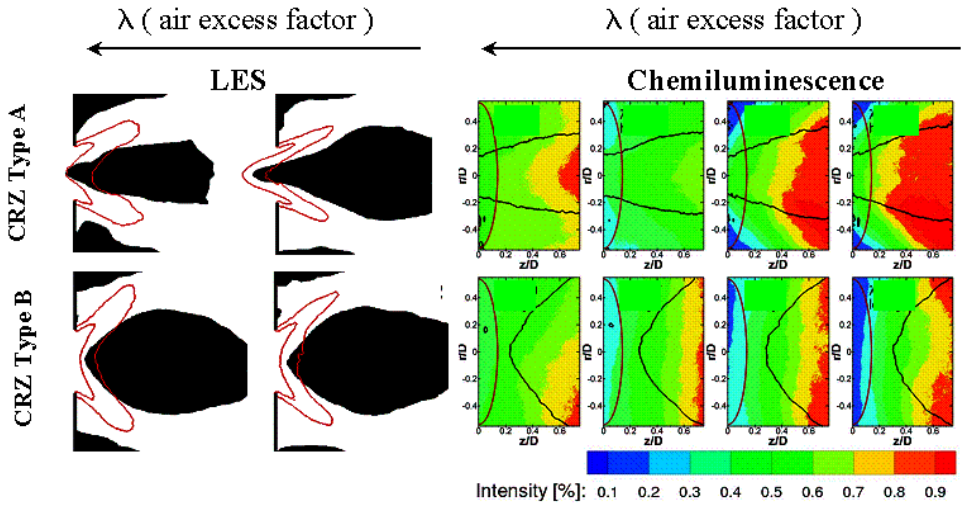

Figure 8: Left: mean flame and CRZ from LES. Right: mean flame and CRZ from CL and PIV on atmospheric test facility

at a fixed flameholder which gives amplification factors decreasing with frequency and not higher than unity. This characteristic is shown both by LES and experiments. LES results however underestimate the amplitude of the experimental FTF by approx a factor half. Explanation of the

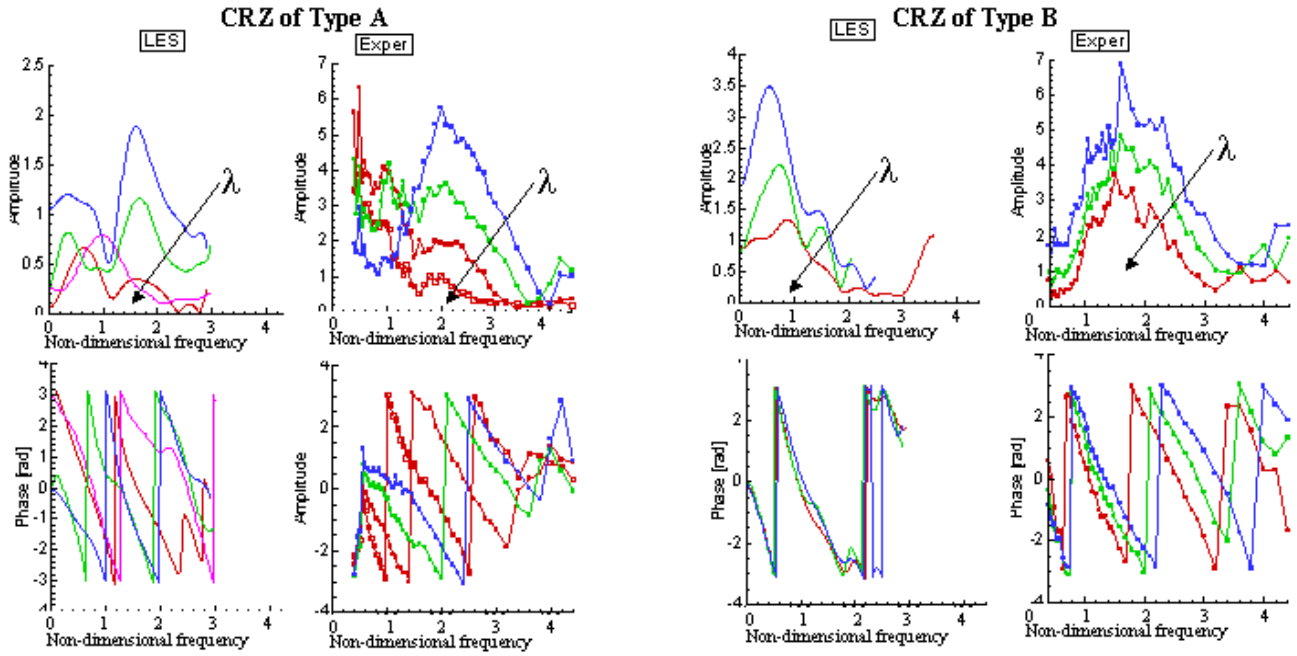

Figure 9: Comparison between experimental and numerical Flame Transfer Functions for flames stabilized at CRZ of type A and type B

observed FTF behaviour is currently in progress. The analysis should concentrate on separating the mechanisms of flame surface area production and turbulent flame speed fluctations as main contributions to fluctuations in reactants consumption rate. In the present work the analysis is limited to a qualitative investigation of the fluctuating axial velocity and progress variable fields decomposed with Proper Orthogonal Decomposition. Consistency with the FTF is obtained by applying the Wiener-Hopf filter to the time sequences representing the projection of the flowfield snapshots along the POD modes, i.e. determining the transfer function of the POD modes. Figure

10 shows contours of the most intense POD mode with axial nature. It is assumed in fact that anti-symmetric modes (e.g. precession) do not contribute to the total reactants consumption rate (their net contribution cancels out). In case of CRZ of type A, the most intense axial mode is also the most intense between all POD modes but in case of CRZ of type B, the most intense mode is a precessing one while the most intense axial mode is in third place. All the phase distributions start from π, i.e. in opposition with the inlet forcing. The results lead to two important considerations. First, the most intense axial mode in case of CRZ of type A shows a change of phase with decreasing λ as also observed in the FTFs. In line with the FTFs, this however doesn't happen in case of CRZ of type B. Second, the response (peak value) of the axial velocity mode in case of CRZ of type A is approximately four times larger than the response in case of CRZ of type B. The situation is however reversed for what concerns the response of the progress variable (which directly controls the FTF) which, in case of CRZ of type B is approx ten times higher than in case of CRZ of type A. Given that the flame displacement is connected with the fluctuating velocity field, such a result indicates that in case of CRZ of type A the coupling between flame and CRZ is much weaker than in case of CRZ of type B. This is in line with the flame stabilization analysis carried out in [13] where it was shown that flames stabilized at narrow CRZ do not typically attach to the apex of the CRZ but instead position themselves more downstream. On the other hand, the more flat is the CRZ at its apex as seen with CRZ of type B, the more the flame moves upstream and increase its coupling with the CRZ apex. In conclusion the CRZ of type B responds to the forcing more weakly than the CRZ of type A but given the stronger flame - CRZ coupling, its FTF shows higher amplitude values.

4 Conclusions

It has been shown that low emission flames stabilized at the CRZ produced via the mechanism of vortex breakdown have dynamic characteristics strongly depending from the structure of the CRZ. From an aerodynamic point of view, a transition between two CRZs has been observed: type A, narrow CRZ with apex in the burner and type B, flat CRZ with apex in the combustor.

Flames stabilized at the CRZ of type A have been found to respond more weakly to an inflow perturbation in air mass flow rate than flames stabilized at the CRZ of type B. A possible explanation of this behaviour is provided by the transfer function of the coherent structures identified via a Proper Orthogonal Decomposition. Despite the response of the CRZ of type A to the forcing is larger than in case of CRZ of type B, the response of the progress variable field is weaker. This behaviour correlates well with the flame stabilization properties presented in [13] which suggest a flame-CRZ coupling in case of CRZ of type B stronger than in case of CRZ of type A.

References

[1] Rayleigh, J. W. S., *The Theory of Sound*, New York, 1945.

[2] V. Bellucci, Modeling and Control of Gas Turbine Thermoacoustic Pulsations, PhD Thesis Technischen Universität Berlin 2009

[3] Schuermans, B.B.H., Paschereit, C.O., Polifke, W., and Van der Linden, J.H., 2000, Prediction of the acoustic pressure spectra in Gas Turbines based on measured transfer matrices, ASME Turbo Expo '00, May 8-11,2000.

[4] Crocco L. Aspects of combustion instability in liquid solid propellant rocket motors. Part I. *Journal of the American Rocket Society*, **21**, 163178 (1951)

[5] A.P. Dowling, A kinematic model of a ducted flame, *J. Fluid Mech.* **394**, 5172, (1999)

[6] G. Borghesi, F. Biagioli and B. Schuermans, Dynamic response of turbulent swirling flames to acoustic perturbations,*Combustion Theory and Modelling* ,**13**:3, 487 512,(2009)

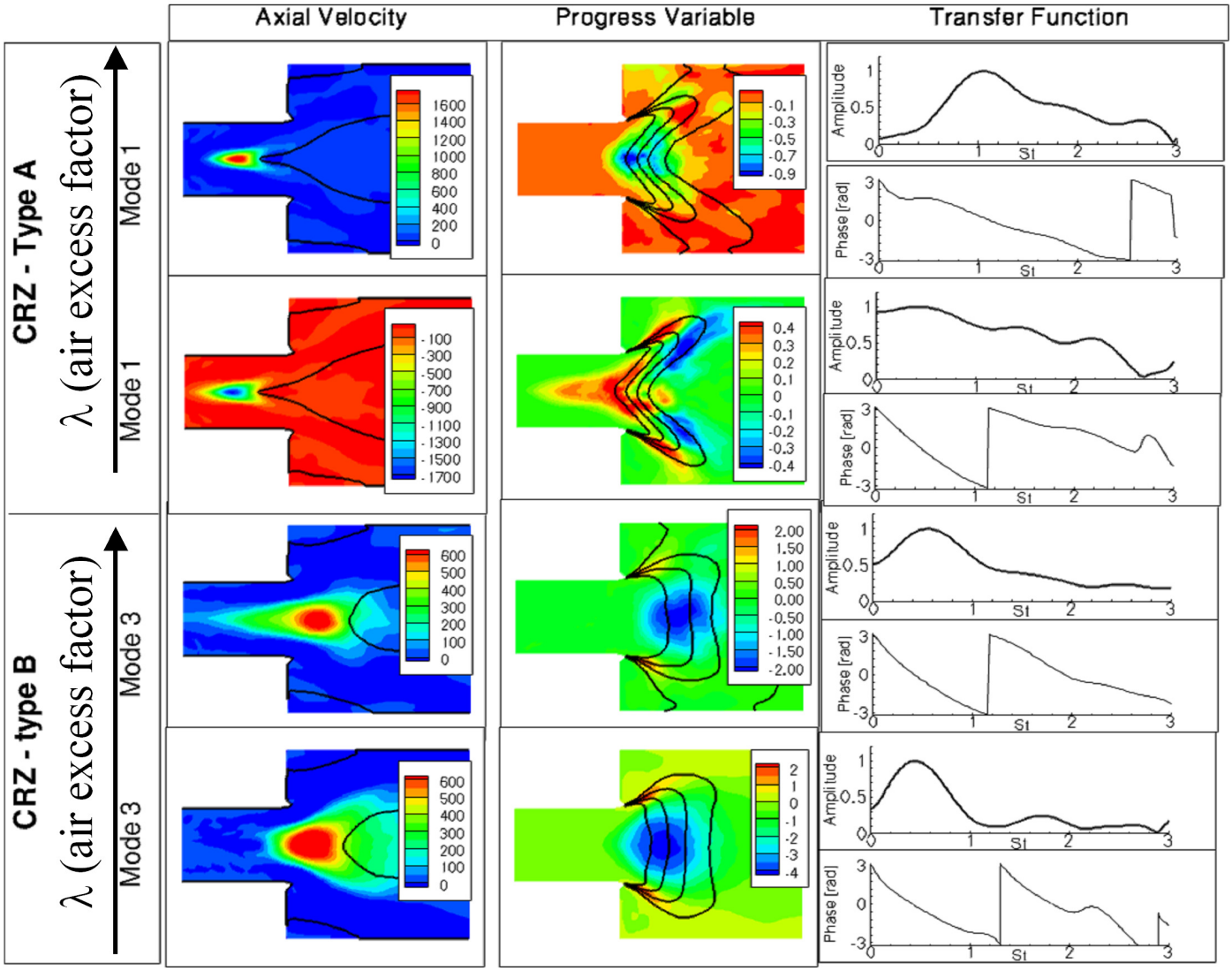

Figure 10: Distribution of POD modes for axial velocity and progress variable. Right: transfer functions of the POD modes time amplitudes

[7] P. Billant, J.-M. Chomaz and P. Huerre, Experimental study of vortex breakdown in swirling jets, *J. Fluid Mech.*, **376**, 183-219, (1998)

[8] G. K. Batchelor. An introduction to Fluid Dynamics. Cambridge University Press, 1967

[9] J. J. Keller, W. Egli, Force and Loss-Free Transitions between Flow States. *Journal of Applied Mathematics and Physics*, **36**,855-, (1985).

[10] Zimont, V.L., *Experimental Thermal and Fluid Science*, **21**, 179186, 2000

[11] Huber, A., Polifke, W., Dynamics of practical premix flames, Part I: Model Structure and Identification; *International Journal of Spray and Combustion Dynamics*, **1**:2, 199-229, (2009).

[12] Paschereit, C., Schuermans, B., Polifke, W., and Mattson, O. a., Measurement of Transfer Matrices and Source Terms of Premixed Flames, ASME 99- GT-0133, Proc. ASME Turbo Expo 1999, Indianapolis, June 7-10., 1999.

[13] F. Biagioli, Stabilization mechanism of turbulent premixed flames in strongly swirled flows *Combustion, Theory and Modelling*, **10**:3, 389-412, (2006)